THE ASTROPHYSICAL JOURNAL, 530:L13–L16, 2000 February 10

HUBBLE SPACE TELESCOPE AND VERY LARGE ARRAY OBSERVATIONS OF THE H_2O GIGAMASER GALAXY TXS 2226−184[1]

HEINO FALCKE,[2] ANDREW S. WILSON,[3,4] CHRISTIAN HENKEL,[2]
ANDREAS BRUNTHALER,[2] AND JAMES A. BRAATZ[5]

Received 1999 November 4; accepted 1999 December 14; published 2000 January 17

ABSTRACT

We present *Hubble Space Telescope*/Wide-Field and Planetary Camera 2 images in Hα + [N II] $\lambda\lambda$6548, 6583 lines and continuum radiation and a VLA map at 8 GHz of the H_2O gigamaser galaxy TXS 2226−184. This galaxy has the most luminous H_2O maser emission known to date. Our red continuum images reveal a highly elongated galaxy with a dust lane crossing the nucleus. The surface brightness profile is best fitted by a bulge plus exponential disk model, favoring classification as a highly inclined spiral galaxy (i = 70°). The color map confirms that the dust lane is aligned with the galaxy major axis and is crossing the putative nucleus. The Hα + [N II] map exhibits a gaseous, jetlike structure perpendicular to the nuclear dust lane and the galaxy major axis. The radio map shows compact, steep spectrum emission that is elongated in the same direction as the Hα + [N II] emission. By analogy with Seyfert galaxies, we therefore suspect that this alignment reflects an interaction between the radio jet and the interstellar medium. The axes of the nuclear dust disk, the radio emission, and the optical line emission apparently define the axis of the active galactic nucleus. The observations suggest that in this galaxy the nuclear accretion disk, obscuring torus, and large-scale molecular gas layer are roughly coplanar. Our classification of the host galaxy strengthens the trend for megamasers to be found preferentially in highly inclined spiral galaxies.

Subject headings: galaxies: active — galaxies: individual (TXS 2226−184) — galaxies: jets — galaxies: nuclei — galaxies: Seyfert — masers

1. INTRODUCTION

In recent years a number of active galaxies have been found to have powerful H_2O maser emission in their nuclei (e.g., Braatz, Wilson, & Henkel 1994, 1996). It is known that the H_2O megamaser phenomenon is associated with nuclear activity since all such megamaser sources are in either Seyfert 2 or LINER nuclei. The standard model for Seyfert galaxies involves a central engine (black hole and accretion disk) producing ionizing radiation and an "obscuring torus" which shadows the ionizing radiation into biconical beams along its rotation axis (see Antonucci 1993 for a review). This beaming is readily seen in some Seyfert galaxies as biconical emission-line structures (e.g., Pogge 1989). Extended radio emission, when present, is usually aligned with the emission-line gas (e.g., Wilson & Tsvetanov 1994). Detailed studies also indicate a strong interaction between the radio ejecta and the optically visible ionized gas (Capetti et al. 1996; Falcke et al. 1996; Falcke, Wilson, & Simpson 1998; Ferruit et al. 1999).

It appears reasonable to infer that the masers trace molecular material associated with the obscuring torus or an accretion disk that feeds the nucleus. This notion was confirmed in great detail by VLBI observations of the megamaser in NGC 4258 (Miyoshi et al. 1995; Greenhill et al. 1995). The positions and velocities of the H_2O maser lines show that the masing region is a thin disk in Keplerian rotation around a central mass of $3.9 \times 10^7\,M_\odot$ at a distance of ≈0.16 pc from that mass (Herrnstein et al. 1999).

Although plausible scenarios for the megamaser phenomenon exist (e.g., Neufeld & Maloney 1995), it is by no means clear how the material that obscures the nucleus (the "obscuring torus") and the masing disk are related. The masing disk may be part of a geometrically thin, molecular accretion disk at smaller radii than the torus or the thin, central plane of a thick torus in which the column density is high enough for strong amplification. Alternatively, the whole structure could be a warped thin disk, so the masing gas might be misaligned with the central accretion disk. The most straightforward picture consistent with current data would, however, have the masing disk, obscuring torus, and any more extended molecular cloud distribution as one coherent accretion structure feeding the central engine, with the ionized thermal and nonthermal radio plasma roughly along the rotation axis.

We have therefore started a program to observe the narrow-line regions (NLRs) of all known megamaser galaxies with the *Hubble Space Telescope* (*HST*) to establish this often suggested link between the molecular disk responsible for the maser emission and the obscuring torus responsible for the ionization cones. We are also obtaining continuum color images to search for the obscuring material directly.

The most luminous known H_2O maser source is found in the galaxy TXS 2226−184[6] (IRAS F22265−1826; Koekemoer et al. 1995) at a redshift of z = 0.025 (luminosity distance D = 101 Mpc for H_0 = 75 km s^{-1} Mpc^{-1} and q_0 = 0.5; in the

[1] Based on observations with the NASA/ESA *Hubble Space Telescope*, obtained at the Space Telescope Science Institute, which is operated by AURA, Inc., under NASA contract NAS5-26555 and on observations made with the VLA operated by NRAO. The National Radio Astronomy Observatory is a facility of the National Science Foundation, operated under a cooperative agreement by Associated Universities, Inc.

[2] Max-Planck-Institut für Radioastronomie, Auf dem Hügel 69, D-53121 Bonn, Germany; hfalcke@mpifr-bonn.mpg.de, chenkel@mpifr-bonn.mpg.de, brunthal@mpifr-bonn.mpg.de.

[3] Astronomy Department, University of Maryland, College Park, MD 20742-2421; wilson@astro.umd.edu.

[4] Adjunct Astronomer, Space Telescope Science Institute.

[5] National Radio Astronomy Observatory, P.O. Box 2, Green Bank, WV 24944; jbraatz@nrao.edu.

[6] The name used by Koekemoer et al. (1995) does not follow the suggested and by now accepted convention used later in the Texas survey (Douglas et al. 1996).

images 0.″1 corresponds to 46 pc). Koekemoer et al. (1995) referred to this object as a gigamaser in view of its isotropic luminosity in the 1.3 cm water line of 6100 ± 900 $L_{\odot}$. In this Letter, we present Hα + [N II] λλ6548, 6583 and broadband continuum observations of TXS 2226−184 obtained with the *HST* and the VLA. Our results indeed show a linear Hα + [N II] structure along the radio axis and perpendicular to a dust lane. This supports the connection between megamaser emission, dusty disk, obscuring torus, and the NLR discussed above. We also classify the host galaxy as a spiral.

2. OBSERVATIONS AND DATA REDUCTION

2.1. *HST Observations*

TXS 2226−184 was observed with the Planetary Camera (PC) on board the *HST* (pixel scale is 0.″0455 pixel^{-1}) in three filters: F814W (red continuum), F547M (green continuum), and F673N (redshifted Hα + [N II] λλ6548, 6583). The total integration times were 120, 320, and 1200 s, respectively, all exposures being split into two or three integrations to allow cosmic-ray rejection. All observations were performed within one orbit on 1998 December 6.

2.2. *HST Data Reduction*

The images were processed through the standard Wide Field Planetary Camera 2 (WFPC2) pipeline data reduction at the Space Telescope Science Institute. Further data reduction was done in IRAF and included cosmic-ray rejection, flux calibration, and rotation to the cardinal orientation. The zero of magnitude for each continuum filter was determined from the *HST* data handbook in the VEGAMAG[7] system. Sometimes we will refer to the red and green continuum filters as *I* and *V*, respectively, even though F547M is not a good match to Johnson-Cousins *V*; an error of 0.2 mag can be expected. For the continuum filters, a constant background level was determined in an emission-free region of the PC (to represent sky brightness) and subtracted from the image. This correction is mainly important for obtaining good color information in faint regions. The galaxy continuum near the Hα + [N II] line was determined by combining the red and green continuum images, scaled to the filter width of F673N and weighted by the relative offset of their mean wavelengths from the redshifted Hα + [N II] emission. The continuum was then subtracted from the on-band image to obtain an image of Hα + [N II]. We did not apply any shifts between the images because they were all taken within one orbit and at the same position on the PC chip. From the two broadband images, we constructed a color map by dividing the green by the red filter image, including only pixels for which the flux was at least 5 times the average noise level in each frame. To increase the signal-to-noise ratio at larger radii, we also computed color maps in which the original image was block averaged by 2 × 2 or 4 × 4 pixels. Each of these maps was also clipped at its 5 σ level and sampled at the PC pixel scale. The three maps were then combined, with each image being weighted by its inverse blocking size. This allows one to have a composite color map in which the bright center is shown at full resolution and the outer, low surface brightness regions (which were clipped in the full resolution map) are seen at lower resolution. This is similar to an unsharp mask technique.

[7] A system in which Vega has magnitude zero in all *HST* filters. The zero points of the canonical Johnson-Cousins system differ from the corresponding *HST* filters by up to 0.02 mag for closely matched filters and up to 0.2 mag for the rest.

2.3. *VLA Observations and Data Reduction*

We observed the galaxy with the VLA in the A configuration at 8.46 and 15 GHz on 1999 August 1 in snapshot mode for 5 minutes and at 4.85 GHz on 1998 May 21 for 10 minutes. We observed a phase calibrator at the beginning and end of the scan and 3C 48 as a flux density calibrator. Using the AIPS software, the data were self-calibrated and maps were produced.

3. RESULTS

3.1. *Radio Map*

A slightly superresolved map of TXS 2226−184 at 8.46 GHz using a circular restoring beam of 0.″2 is shown in Figure 1 (*bottom*), where we have subtracted the central point source to show the extended emission more clearly. The source is resolved with a peak flux density of 15 mJy and a total flux density of 23 mJy. The emission is elongated in P.A. −37° toward the northwest and in P.A. 146° toward the southeast. No further extended emission was detected in our maps. This is also true for lower resolution maps (VLA C and B configuration) at 5 and 8 where the flux densities agree with ours (Golub & Braatz 1998). The total fluxes at 4.85 and 14.94 GHz are 37 and 13 mJy, respectively. At these frequencies, the source is extended in the same direction as at 8.46 GHz. If we compare our total flux densities with the flux density the galaxy had in the Texas survey at 365 MHz (198 mJy; Douglas et al. 1996), we find the spectrum to be steepening from $\alpha = -0.65$ ($S_{\nu} \propto \nu^{\alpha}$) between 365 MHz and 4.85 GHz to $\alpha = -1$ between 8.46 and 14.94 GHz. Because of the compact structure, this steepening is most likely not due to resolution effects. The position of the central radio component is $\alpha = 22^{h}26^{m}30\overset{s}{.}07$, $\delta = -18°26'09\overset{''}{.}6$ (B1950).

3.2. *HST Images*

Our *HST* images are shown in Figure 1. The continuum map, which is the combination of the red and green filters used also for off-band subtraction, reveals a highly elongated galaxy along P.A. 55°. The inner region (1″ diameter) is bisected by a dark band, presumably a nuclear dust lane. We have fitted an elliptical Gaussian function to the inner region to locate the centroid of the continuum emission. The centroid thus found is marked with a cross in Figure 1, and we shall refer to this position as the "nucleus" of the galaxy. It is in the middle of the supposed dust lane. The presence of this dust lane is further strengthened by the color map, which shows a region of high reddening along P.A. 60° extending roughly 1″ across the nucleus. We also see higher reddening on the northwest side of the galaxy than on the southeast which, for a disk galaxy, would indicate that the northwest side is the nearer side of the galaxy disk (Hubble 1943).

The Hα + [N II] map shows a highly elongated structure roughly along P.A. −40° ± 5°, i.e., in the same direction as the radio emission, with a bright spot 0.″2 northwest of the supposed nucleus. The emission extends further toward the southeast, with a broad, "wiggly" structure near the nucleus and a "plume" 1.″5 from the nucleus. As in the continuum image, the adopted nucleus is not very bright in Hα + [N II], presumably because of obscuration by the dust lane.

The adopted nucleus in the *HST* images is within 1.″5—the typical error in absolute *HST* astrometry—of the radio nucleus. Therefore, we have assumed that the optical and radio nuclei coincide and have shifted the *HST* images accordingly (see Falcke et al. 1998 for a discussion of VLA/*HST* registration

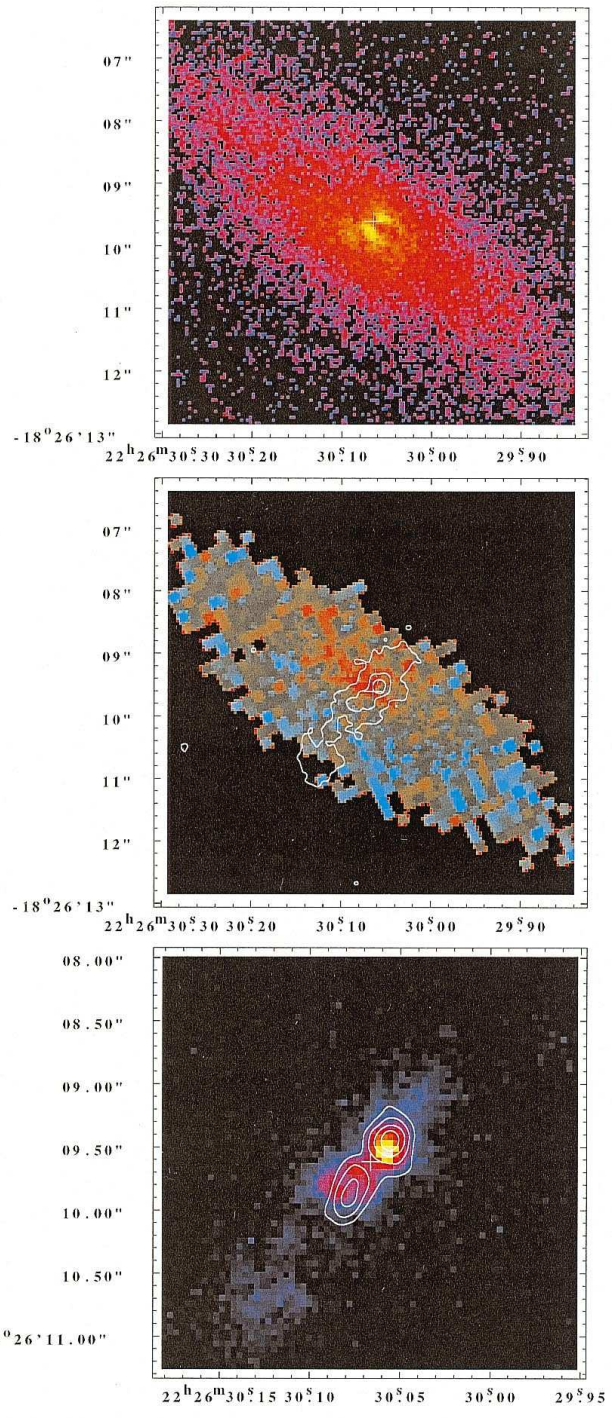

FIG. 1.—*Top:* Continuum map obtained by averaging the red and green images taken with the Planetary Camera (0.″0455 pixel size). The centroid of the continuum in the inner part of the galaxy (see text) is marked here and in the following panels by a cross, and the B1950 coordinates are from the VLA astrometry (assuming the radio nucleus and the optical centroid are coincident). *Middle:* Color map obtained by dividing the green by the red continuum image (same spatial scale as top). The flux density ratio ranges from 0.4 (*red colors*) to 1.5 (*blue colors*) which roughly corresponds to $V-I$ colors ranging from 2.2 to 0.8. The gray areas are around $V-I \sim 1.3$. Contours overlaid are of the Hα + [N II] image (*bottom*). *Bottom:* Continuum-subtracted Hα + [N II] image of TXS 2226−184. The Hα + [N II] flux in a rectangular 1.″7 × 3.″2 aperture is 2.5×10^{-14} ergs s^{-1} cm^{-2}, and the intensity scale is proportional to the square root of the brightness. Contours overlaid are of the 8.46 GHz VLA radio continuum (contours starting at 0.3 mJy and increasing by factors of $\sqrt{2}$). We have subtracted the central point source from the radio map to show the extended structure more clearly.

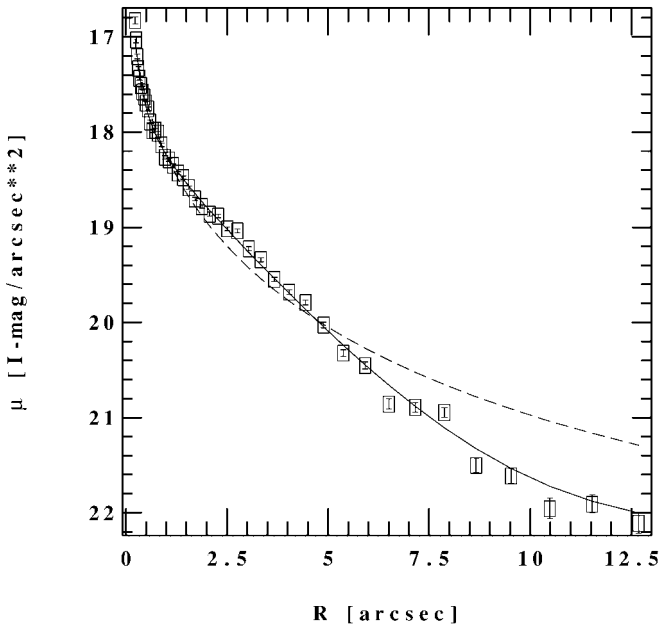

FIG. 2.—Surface brightness μ of TXS 2226−184 in the F814W filter (I band) as a function of the semimajor axis in arcseconds. The solid line is a disk galaxy fit with both bulge and disk components, as described in the text. The dashed line is a fit with only a bulge component.

and errors). The coordinates given in Figure 1 are after this shift has been performed.

In the larger field of view of all four WFPC2 chips, we find a number of faint, extended sources around TXS 2226−184 that are probably galaxies. In particular, there is a highly elongated galaxy only 17.″2 southwest (P.A. = −120°) of the nucleus of TXS 2226−184 at $\alpha = 22^{h}26^{m}29\overset{s}{.}0$, $\delta = -18°26'18\overset{''}{.}3$ (B1950).

3.3. *Isophotes and Radial Profile Fitting*

We have fitted elliptical isophotes to the red continuum image of the galaxy ignoring the innermost few pixels which are heavily affected by the dust lane. The center was fixed at the adopted nucleus (see § 3.2). The ellipticity is close to zero at $R \simeq 0\overset{''}{.}5$, below which it is strongly affected by the dust lane, and approaches a constant value of around 0.6 beyond $R \gtrsim 3''$. Similarly, the P.A. of the semimajor axis changes rapidly from 140° to a value of 65° at 0.″5 and stays essentially constant (at 50°–60°) at larger radii. The colors are relatively red in the inner region, dropping from $V-I \sim 1.65$ to around 1.35 at the outer isophotes.

Figure 2 shows the azimuthally averaged surface brightness of the isophotes as a function of R. This profile was fitted in IRAF with (1) an exponential disk profile,

$$S_{\rm disk} = S_0 \exp\left(-\frac{R}{R_0}\right), \qquad (1)$$

plus a bulge component (de Vaucouleurs 1948),

$$S_{\rm bulge} = S_e \exp\left\{-7.688\left[\left(\frac{R_{\rm SMA}}{R_e}\right)^{1/4} - 1\right]\right\}, \qquad (2)$$

to represent a spiral or S0 galaxy, and (2) with a bulge component (eq. [2]) only to represent an elliptical galaxy. While the fitting was done using surface brightness S weighted by

the inverse errors, we give the results in the more conventional form of surface brightness μ (in units of mag arcsec^{-2}).

For the disk plus bulge model (fitting 1), we obtained a good fit (reduced $\chi^2 = 0.86$) with the parameters $\mu_0 = 18.0$ mag arcsec^{-2}, $R_0 = 2\farcs4$ (1.1 kpc), $\mu_e = 19.7$ mag arcsec^{-2}, and $R_e = 0\farcs6$ (0.29 kpc). For a bulge component only (fitting 2), i.e., an elliptical galaxy profile, the fit is much worse (reduced $\chi^2 = 4.9$) and at large radii lies consistently above the data (Fig. 2). The parameters we get here are $\mu_e = 22.8$ mag arcsec^{-2} and $R_e = 22\farcs7$ (10.5 kpc). The results clearly favor a spiral over an elliptical galaxy. The ellipticity of TXS 2226−184 ($e = 1 - b/a = 0.61$ at $2\farcs7 < R < 6\farcs0$) indicates an inclination of the galaxy to the line of sight of 70° (using $i = \arcsin\{[1 - (b/a)^2]/0.96\}^{1/2}$; e.g., Whittle 1992). The details of the fitting depend somewhat on how much of the inner region is excluded, while the preference of a disk plus bulge model over a bulge-only model does not.

The difference between the magnitudes of the integrated bulge and the galaxy as a whole in our spiral galaxy model (see Simien & de Vaucouleurs 1986) is $\Delta m_t = 1.9$ if we integrate along elliptical isophotes with $e = 0.61$. To correct for the inclination-dependent absorption (e.g., Tully et al. 1998), we would have to add ~0.5 mag to obtain the face-on value of this difference. Figure 2 and equation (4) of Simien & de Vaucouleurs (1986) then would formally indicate that TXS 2228−184 is probably an Sb/c (RC2 Hubble type $T = 4$–5). However, this determination of the relative bulge luminosity and the Hubble type classification is very uncertain. Still, our data should be good enough to indicate that TXS 2228−184 is later than S0. The fact that we are measuring at *I* (Simien & de Vaucouleurs use *B*) strengthens this point, since one would expect the bulge to be more prominent relative to the disk at *I* than at *B*. If we integrate our surface luminosity profile to infinity, the total *I* magnitude of disk and bulge is 15.1 mag. The uncertainty in the cutoff radius due to a low signal-to-noise ratio in the outer isophotes may allow an increase of this value by up to 0.4 mag.

4. DISCUSSION AND SUMMARY

Koekemoer et al. (1995) have classified this galaxy as an elliptical or S0 and speculated whether the unusually broad line width of the megamaser emission seen in this galaxy and in NGC 1052 might be typical of elliptical galaxies. Our *HST* images reveal that TXS 2226−184 is almost certainly not an elliptical, so NGC 1052 is the only known megamaser in an elliptical galaxy (Braatz et al. 1994; see also Henkel et al. 1998). On the other hand, the high inclination of TXS 2226−184 strengthens the tentative conclusion of Braatz, Wilson, & Henkel (1997) that megamasers are preferentially found in highly inclined galaxies. Six out of 14 spiral galaxies in their detected megamaser sample have now an inclination $i > 69°$. This excess suggests that nuclear and large-scale dust disks in many active spiral galaxies are indeed related.

The NLR in TXS 2226−184 is very elongated and reminiscent of the jetlike NLR seen in many Seyfert galaxies, as imaged by *HST* (e.g., Capetti et al. 1996; Falcke et al. 1998). These gaseous structures are believed to be produced in the interaction between outflowing radio ejecta and the interstellar medium (e.g., Falcke et al. 1998; Ferruit et al. 1999). The fact that our radio map is elongated along exactly the same direction as the NLR supports this view.

In addition to the NLR and radio jet, we find a dust lane in the nucleus that aligns with the galaxy major axis and presumably represents its normal interstellar medium. The elongation of the NLR and the radio source perpendicular to the northeast-southwest dust lane suggests that the nuclear accretion disk and the obscuring torus are more or less coplanar with the stellar disk in TXS 2226−184. Preliminary results of VLBA observations of the masers in this galaxy indeed seem to roughly show a northeast-southwest orientation along P.A. 20° (L. J. Greenhill 1999, private communication). How to interpret this structure and whether this indicates a warp in the gas disk going from tens of parsec to parsec scales is unclear at present. Further VLBI observations of masers and the continuum in this and other maser sources together with *HST* observations of the host galaxies could help to clarify the nature of the obscuring torus/masing disk and its connection to the large-scale molecular gas structure of the active galactic nucleus host galaxy.

We thank Stacy McGaugh for helpful discussions on galaxy classifications and Lincoln Greenhill for providing information on unpublished VLBA observations of TXS 2226−184. This research was supported by NASA under grant NAG8-1027 and *HST* GO 7278 and by NATO grant SA.5-2-05 (GRG 960086)318/96. H. F. is supported by DFG grants Fa 358/1-1 and 358/1-2.

REFERENCES

Antonucci, R. J. 1993, ARA&A, 31, 473
Braatz, J. A., Wilson, A. S., & Henkel, C. 1994, ApJ, 437, L99
———. 1996, ApJS, 106, 51
———. 1997, ApJS, 110, 321
Capetti, A., Axon, D. J., Macchetto, F., Sparks, W. B., & Boksenberg, A. 1996, ApJ, 469, 554
de Vaucouleurs, G. 1948, Ann. d'Astrophys., 11, 247
Douglas, J. N., Bash, F. N., Bozyan, F. A., Torrence, G. W., & Wolfe, C. 1996, AJ, 111, 1945
Falcke, H., Wilson, A. S., & Simpson, C. 1998, ApJ, 502, 199
Falcke, H., Wilson, A. S., Simpson, C., & Bower, G. A. 1996, ApJ, 470, L31
Ferruit, P., Wilson, A. S., Falcke, H., Simpson, C., Pécontal, E., & Durret, F. 1999, MNRAS, 309, 1
Golub, J. S., & Braatz, J. A. 1998, AAS Meeting, 193, 0612
Greenhill, L. J., Jiang, D. R., Moran, J. M., Reid, M. J., Lo, K. Y., & Claussen, M. J. 1995, ApJ, 440, 619
Henkel, C., Wang, Y. P., Falcke, H., Wilson, A. S., & Braatz, J. A. 1998, A&A, 335, 463
Herrnstein, J. R., et al. 1999, Nature, 400, 539
Hubble, E. 1943, ApJ, 97, 112
Koekemoer, A. M., Henkel, C., Greenhill, L. J., Dey, A., van Breugel, W., Codella, C., & Antonucci, R. 1995, Nature, 378, 697
Miyoshi, M., Moran, J. M., Herrnstein, J., Greenhill, L. J., Nakai, N., Diamond, P., & Inoue, M. 1995, Nature, 373, 127
Neufeld, D. A., & Maloney, P. R. 1995, ApJ, 447, L17
Pogge, R. W. 1989, ApJ, 345, 730
Simien, F., & de Vaucouleurs, G. 1986, ApJ, 302, 564
Tully, R. B., Pierce, M. J., Huang, J.-S., Saunders, W., Verheijen, M. A. W., & Witchalls, P. L. 1998, AJ, 115, 2264
Whittle, M. 1992, ApJS, 79, 49
Wilson, A. S., & Tsvetanov, Z. I. 1994, AJ, 107, 1227